Schweizerische Eidgenossenschaft
Confédération suisse
Confederazione Svizzera
Confederaziun svizra

Eidgenössisches Departement für
Umwelt, Verkehr, Energie und Kommunikation UVEK

Bundesamt für Energie BFE

Jahresbericht 27. November 2009

Efficient direct conversion of heat into electricity by innovative layered structures

Layered Thermoelectric Converters (LTEC)

Auftraggeber:
Bundesamt für Energie BFE
Forschungsprogramm Elektrizitätstechnologien & -anwendungen
CH-3003 Bern
www.bfe.admin.ch

Auftragnehmer:
EMPA
Department of Solid State Chemistry and Catalysis
Überlandesstrasse 129
CH-8600 Dübendorf
www.empa.ch/abt131

Autoren:
Dimas Surya Alfaruq, EMPA, dimas.alfaruq@empa.ch
Anke Weidenkaff, EMPA, anke.weidenkaff@empa.ch

BFE-Bereichsleiter: Dr. Michael Moser
BFE-Programmleiter: Roland Brüniger
BFE-Vertrags- und Projektnummer: 153459 /102669

Für den Inhalt und die Schlussfolgerungen ist ausschliesslich der Autor dieses Berichts verantwortlich.

Abstract

Thermoelectric materials are developed for direct conversion technologies of heat into electricity. Perovskite-type oxides are promising candidates for high temperature thermoelectric applications because their properties can be easily controlled by suitable modifications in their composition (s. PhD thesis Rosa Robert).

To improve the thermoelectric properties nanostructured *n*-type thermoelectric perovskite phases $CaMn_{1-x}Nb_xO_{3\pm\delta}$ (x = 0.01; 0.03; 0.05; 0.07; 0.10) were synthesized by a soft chemistry method. The morphology was studied by SEM. The crystallographic structure was determined by X-ray powder diffraction (XRPD). The high temperature thermoelectric properties (Seebeck coefficient, electrical resistivity and thermal conductivity) were compared.

The focus of this work is to investigate the effect of Nb^{5+} substitution for Mn^{4+} on the B-site of the ABX_3 crystal structure on the thermoelectric performance given by the ZT values.

Project goals

Wast heat losses are a major problem regarding the fuel economy of combustion engines. Ideally, this heat could directly be converted into electricity by thermoelectric devices which would increase the efficiency of the engines.

A measure for evaluating the thermoelectric efficiency of a material is the Figure of Merit ZT. ZT is defined as $ZT = S^2T\sigma / \kappa$, where S is the Seebeck coefficient, T the absolute temperature, σ the electrical conductivity, and κ the thermal conductivity [12]. Good thermoelectric materials should have a high Seebeck coefficient, high electrical conductivity, and low thermal conductivity.

Perovskite-type oxides are interesting materials for thermoelectric applications as their properties can be easily *fine-tuned* by substituting ions in the structure. According to the respective requirements, materials with insulating, semiconducting (p-type or n-type), metallic or even superconducting transport properties can be manufactured [12].

Perovskite manganates are well known for their high magneto resistance which can be explained by the double exchange (DE) model [3]. Calcium manganate, $CaMnO_3$, is an antiferroelectric insulator that posses high thermopower values. Appropriate substitution at its A- or B-site can transform the calcium manganate into a semiconducting material, though. Introduction of Nb^{5+} into the Mn^{4+} matrix increases the charge carrier concentration. Based on the Jahn-Teller-Theory, substitution of $Mn^{4+}(e_g^0 t_{2g}^3)$ by Nb^{5+} in $CaMnO_3$ induces the formation of Mn^{3+} $(e_g^1 t_{2g}^3)$ due to charge equalization in the system. Electrons in the e_g orbitals act as mobile charge carriers in the Mn^{4+}-O-Mn^{3+} framework resulting in *electron hopping* [3] conduction.

The thermal conductivity of a material can be reduced in several ways: (i) by introducing heavy elements such as Niobium, Lanthanum, or Molybdenum since high atomic weight elements display smaller phonon energies, lower speed of sound and thus lower intrinsic thermal conductivity compared to light elements [6]; (ii) generating complex crystal structures with many atoms per unit cell and rattles in the lattice (introducing atoms that move freely in the lattices) [6]; (iii) lowering the structural dimension to e.g. nanoscale, thin films or superlattices. Particularly, in thin films size effects on the thermal conductivity become important as the mean free path of the phonons decreases with decreasing thickness of the film. This results in increased boundary scattering which reduces thermal transport and, therefore, the thermal conductivity of the material. In this respect, layered thermoelectric converters are promising candidates for efficient thermoelectric power production because of increased phonon scattering [11].

In the present study, our goal was to substitute Mn in $CaMnO_3$ with a variety of Nb concentrations (0.01;0.03;0.05;0.07;0.10) in order to investigate the influence of Nb substitution on the ZT value. $CaMnO_3$ doped with Nb at the B-site was chosen because previous studies showed a relatively high ZT value of 0.32 at 2% Nb substitution was found in previous studies in a former project (PhD thesis Laura Bocher).

A soft chemistry (SC) synthesis method [9] instead of a solid state reaction (SSR) method was used because smaller grain sizes can be achieved. The applied SC method consisted in the preparation of complex precursors where citric acid is used as chelating agent for the involved cations. In this way, particle sizes at the nanoscale (50-130 nm in diameter) can be synthesized creating more scattering sites for phonons and, consequently, leading to lower thermal conductivities. What is more, the SC method offers the advantage of a low temperature synthesis route that allow the preparation of a variety of compositions including highly reactive metastable phases that can not be achieved by classical SSR methods [3].

Here the precursor chemistry will be improved to enable on the one hand side the upscale of the synthesis process for the TOM production (see project TOM) and on the other hand side to develop a precursor system for the thin film production.

As a next step, we will grow single crystals from the Nb-doped $CaMnO_3$ compound that revealed the best ZT value. Single crystal growth will be performed in a Floating Zone Furnace (Crystal System Corp) to rule out influences of grain boundaries on the PF- values.

Experiments and results

1. Experimental

The perovskite-type samples $CaMn_{1-x}Nb_xO_3$ (x=0.01; 0.03; 0.05; 0.07; 0.10) were prepared from stoichiometric amounts of $Ca(NO_3)_2{\cdot}4H_2O$, $Mn(NO_3)_2{\cdot}4H_2O$, and $NbCl_5$ using a soft chemistry method with citric acid as a chelating agent. All starting materials were dissolved in distilled water with exception of $NbCl_5$ (dissolved in ethanol) prior to mixing. Subsequently, the solution was polymerized at 80-90 °C for 3-4 hours. The polymerization product was heated from 100°C to 300°C overnight at a rate of 20°C/hour. The obtained xerogel was crushed and calcined at a rate 5°C/min from 200°C to a final temperature of 800°C. The samples were pressed into pellets and sintered at 1200°C for 5h. The phase purity of sample was analyzed by a Phillips X'Pert PRO MPD Θ-Θ System equipped with a linear detector X'Celerator. Rietveld refinements were performed using the GSAS program. Seebeck coefficient, electrical conductivity and power factor of samples were measured using a RZ2000i unit. The morphology of the samples was determined by SEM. Thermal diffusivities, Cp, and oxygen content were measured by LFA, DSC and TGA, respectively. The details of the experimental procedures are explained elsewhere [8], [10].

2. Results and Discussions

2.1. Xray powder diffractograms (XRPD) and SEM pictures

XRPD was used to determine the phase purity of the samples. Figure 1 shows the XRPD and SEM figures of $CaMn_{1-x}Nb_xO_{3\pm\delta}$ (x=0.01;0.03;0.05;0.07;0.10). The samples are pure with no evidence of secondary phases.

SEM images reveal that the soft chemistry synthesis method produces nano-sized particles which agglomerate on top of each other.

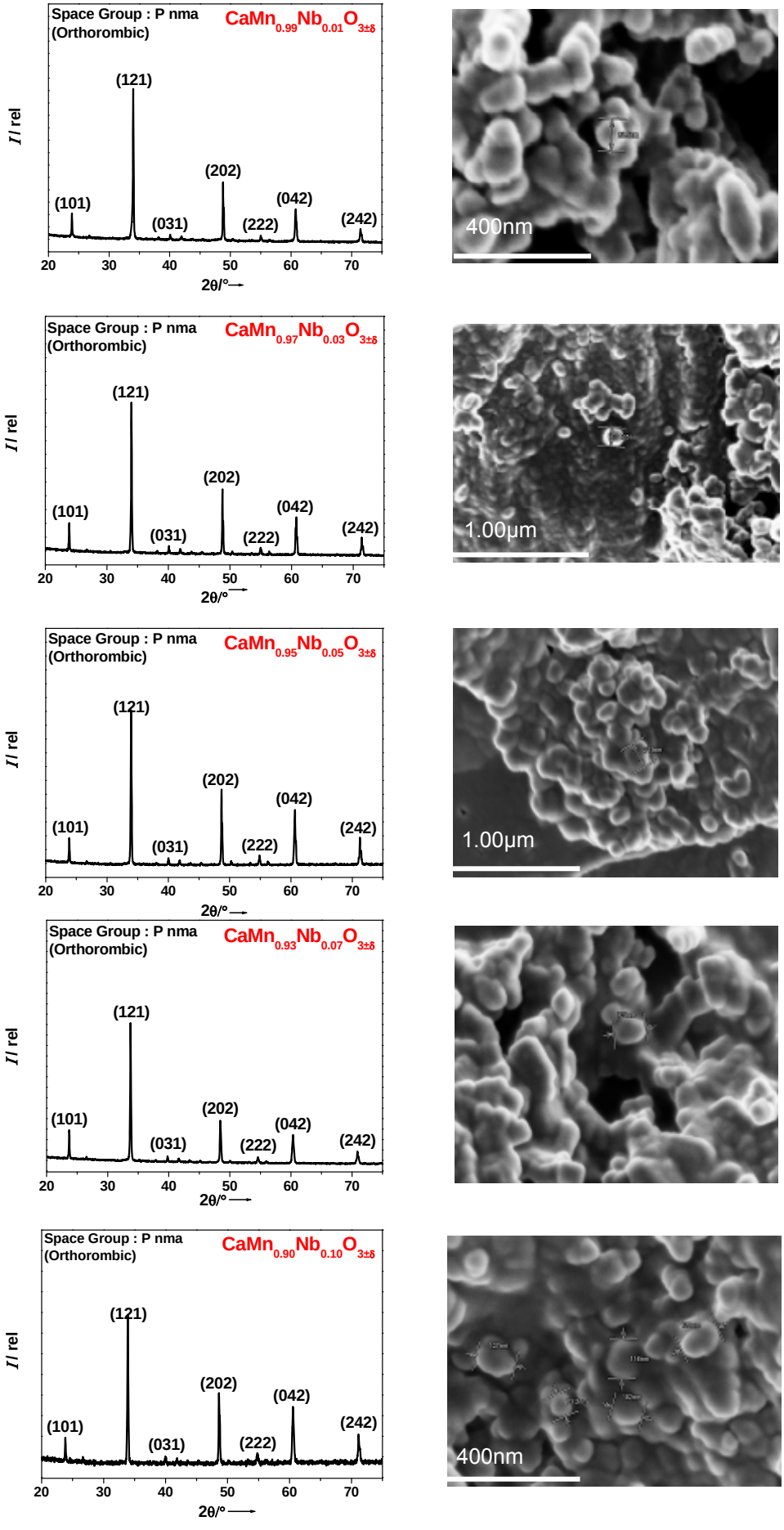

Figure 1: XRP diffractograms and SEM figures of $CaMn_{1-x}Nb_xO_{3\pm\delta}$ (x=0.01;0.03;0.05;0.07;0.10)

2.2. Seebeck Coefficient

Figure 2 shows the correlation between Seebeck coefficient and absolute temperature. It can be seen that with increasing substitution of Mn with Nb, the Seebeck value decreases. This is in agreement with Heikes Formula,

$$S = -\frac{\kappa_B}{e} \ln\left[\frac{(1-x)}{x}\right]$$

where K_B is the Boltzmann constant, *e* is the absolute value of the elementary charge, and x is the charge carrier concentration. As shown in Figure 3, the highest value for the Seebeck coefficient (-270 µV/K) is measured at 1% Nb substitution and the lowest (-110 µV/K) at 10% Nb substitution.

With increasing temperature the Seebeck coefficient also increases reaching a maximum at 1000 K. This is due to a slight reduction of the oxygen content at higher temperatures, leading to excess positive charge and thus to higher Seebeck coefficients.

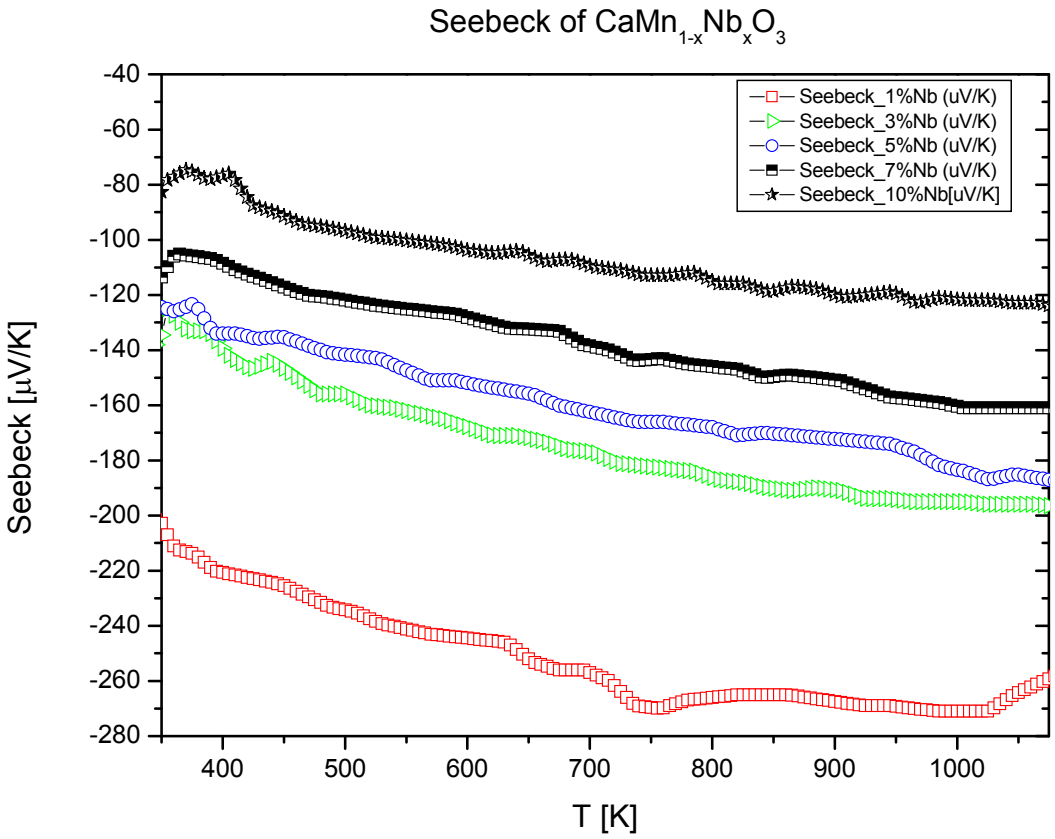

Figure 2: Temperature dependence of the Seebeck coefficients of $CaMn_{1-x}Nb_xO_{3-\delta}$

2.3. Electrical Resistivity

Figure 3 shows the temperature dependence of the electrical resistivity. At 300 K, electrical resistivities of the samples indicate metallic behavior. The values decrease with increasing doping of $CaMnO_3$ with Nb. due to an increase in charge carrier concentration. With increasing temperatures the electrical resistivities of the samples increase. This is in accordance with the metallic behavior and described by the *Bloch-Grüneisen* formula,

$$\rho(T) = \rho(0) + A\left(\frac{T}{\Theta_R}\right)^n \int_0^{\frac{\Theta_R}{T}} \frac{x^n}{\left(e^x - 1\right)\left(1 - e^{-x}\right)} dx$$

where ρ(0) is the residual resistivity due to defect scattering and depends not only on the type of the metal but also on its purity, A is a constant that depends on the electron velocity at the Fermi surface, the Debye radius and the electron density, Θ_R is the Debye temperature as obtained from resistivity measurements and matches closely with the values obtained from specific heat measurements, n is integer and depends on the nature of interaction:

- n=5 implies that the resistance is due to scattering of electrons by phonons (as it is the case for metals)
- n=3 implies that the resistance is due to s-d electron scattering (as it is the case for transition metals)
- n=2 implies that the resistance is due to electron-electron interaction.

When the temperature exceeds 1000 K, the resistivity decreases ($\frac{d\rho}{dT} < 0$) indicating semiconducting properties.

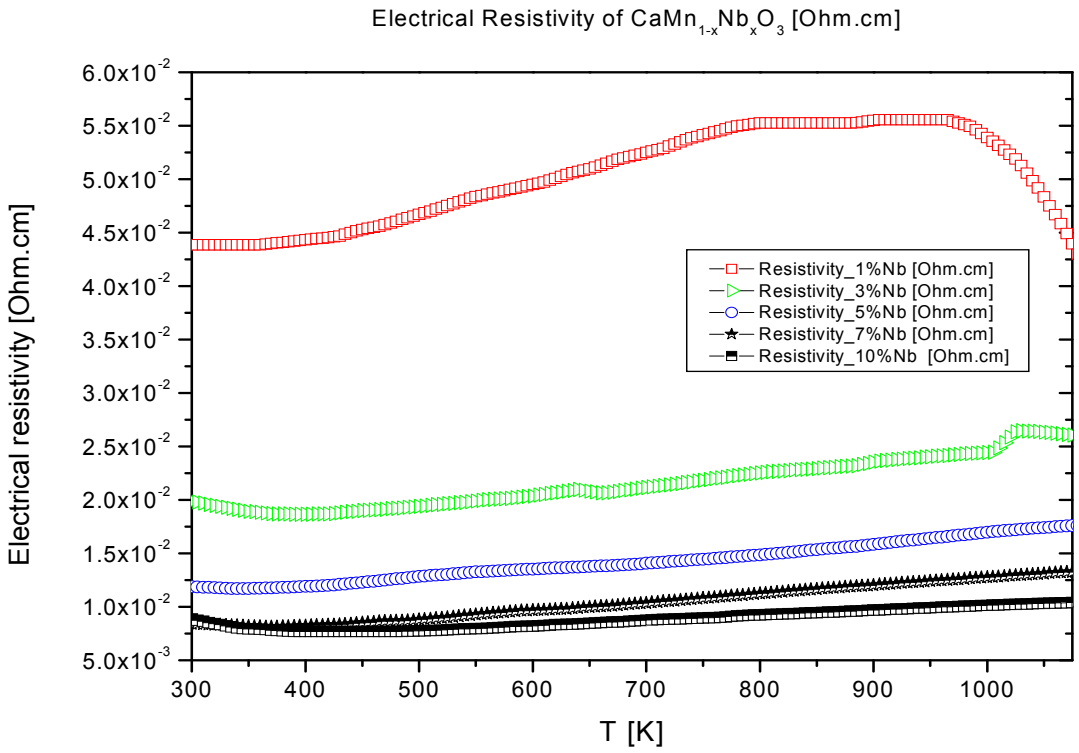

Figure 3: Temperature dependence of the electrical resistivities of $CaMn_{1-x}Nb_xO_{3-\delta}$

2.4. Total Thermal Conductivity

The total thermal conductivity describes the ability of a material to conduct heat. It follows the relation

$$\kappa_{total} = \kappa_{el} + \kappa_{lat}$$

where κ_{el} is the electronic thermal conductivity and $\kappa_{lattice}$ is the lattice thermal conductivity. The temperature dependence of the total thermal conductivity of the compounds is represented in Figure 4. The diagram shows that all samples possess a high total thermal conductivity, being highest for the compound $CaMn_{0.99}Nb_{0.01}O_3$ and lowest for $CaMn_{0.97}Nb_{0.03}O_3$.

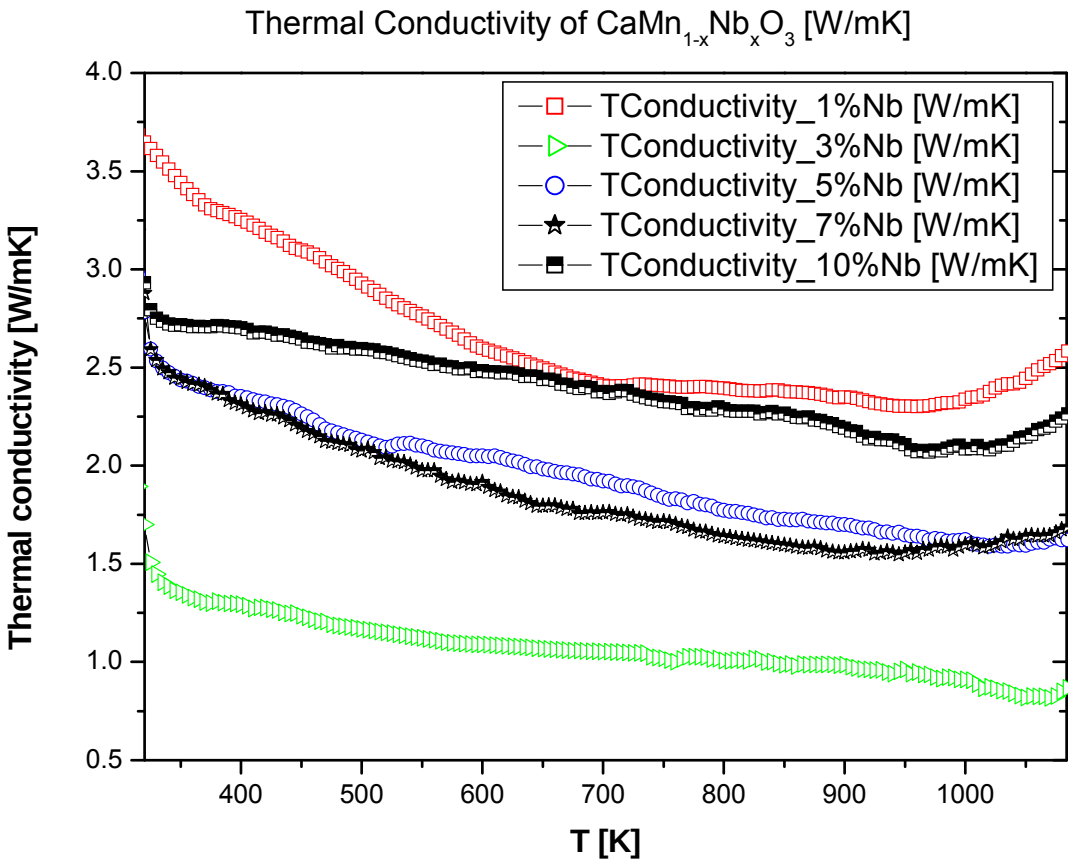

Figure 4: Temperature dependence of the total thermal conductivities of $CaMn_{1-x}Nb_xO_{3-\delta}$

In oxide materials the lattice contribution of the thermal conductivity predominates. The electronic component, though, increases with increasing charge carrier concentration and, hence, with increasing Nb substitution in $CaMnO_3$, as well as with increasing temperature.

The thermal conductivity of the samples depends on their density. Table 1 reveals that the compound with 3% Nb substitution has the lowest density resulting in a lower thermal conductivity compared to the other samples. More research applying a single crystal as a standard is required to investigate the interaction of density and thermal conductivity.

0.01 Nb	0.03 Nb	0.05 Nb	0.07 Nb	0.10 Nb
3.978 (~88%)	2.499 (~60%)	3.944 (~87%)	4.03 (~90%)	4.06 (~90%)

Table 1: Densities of $CaMn_{1-x}Nb_xO_{3-\delta}$ in [g/cm^3] and the percentage of the theoretical value.

2.5. Figure of Merit

In Figure 5, the calculated ZT values of all samples are plotted against temperature. It can be seen that the highest value is achieved for $CaMn_{0.97}Nb_{0.03}O_{3-\delta}$ with $ZT_{1000K} = 0.19$.

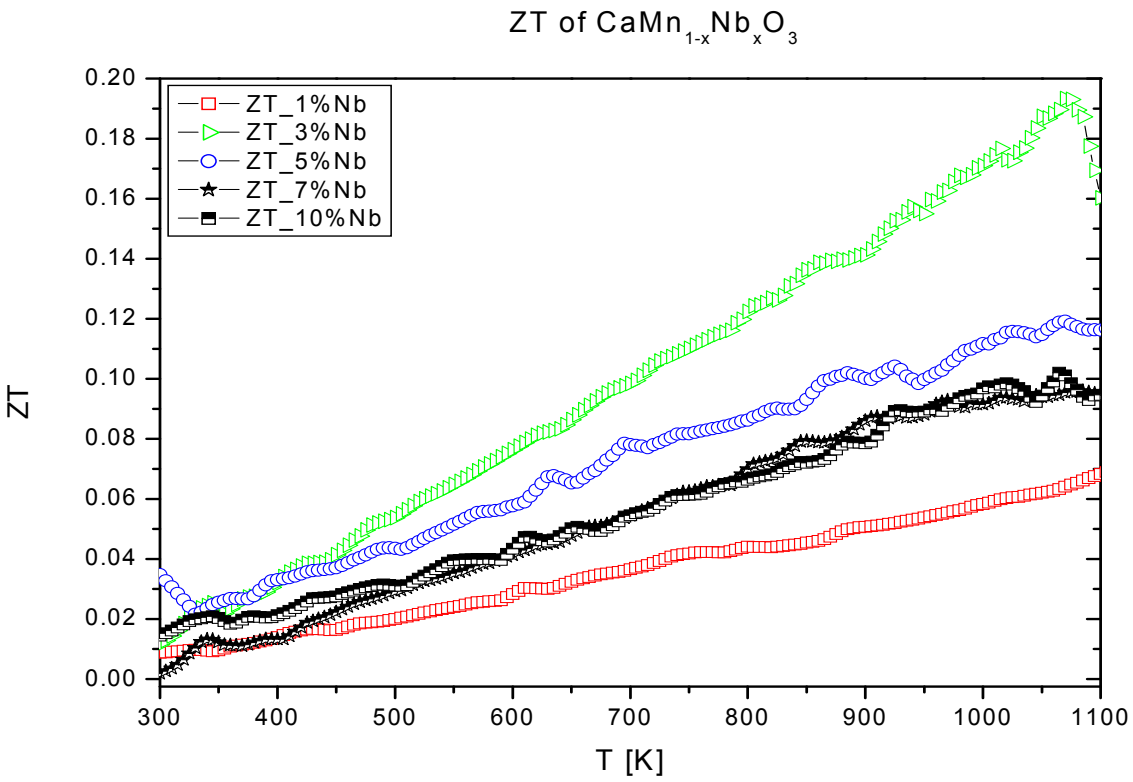

Figure 5: Temperature dependence of the Figure of Merit ZT of $CaMn_{1-x}Nb_xO_{3-\delta}$

A 9.61% mass reduction for $CaMn_{0.97}Nb_{0.03}O_{3-\delta}$ was measured by the oxygen content analysis by TGA/STA (Table 2). This is less than the theoretically expected value of 11.1%. Thus, the exact composition of the compound is calculated to be $CaMn_{0.97}Nb_{0.03}O_{2.85}$ rather than $CaMn_{0.97}Nb_{0.03}O_3$.

0.01 Nb	0.03 Nb	0.05 Nb	0.07 Nb	0.10 Nb
2.968	2.858	2.950	2.874	2.999

Table 2: Oxygen content of $CaMn_{1-x}Nb_xO_{3\pm\delta}$

The amount of Mn^{3+} is the determining factor for the electron hopping effect. The calcium manganese compound with 3% Nb substitution has the highest Mn^{3+} concentration due to oxygen deficiency and, thus, the highest charge carrier concentration.

- $CaMn^{3+}_{0.074}Mn^{4+}_{0.916}Nb_{0.01}O_{2.968}$
- $CaMn^{3+}_{0.33}Mn^{4+}_{0.64}Nb_{0.03}O_{2.858}$
- $CaMn^{3+}_{0.15}Mn^{4+}_{0.8}Nb_{0.05}O_{2.950}$
- $CaMn^{3+}_{0.322}Mn^{4+}_{0.608}Nb_{0.07}O_{2.874}$
- $CaMn^{3+}_{0.102}Mn^{4+}_{0.798}Nb_{0.10}O_{2.968}$

Conclusions for 2009 and Outlook 2010

Substitution of Mn^{4+} by Nb^{5+} in smaller increments offers a good way to investigate the effect of doping on the thermoelectric properties of n-type $CaMnO_3$.

Increasing Nb substitution in the $CaMnO_3$ lattice leads to higher Seebeck coefficients and lower electrical resistivities at low temperatures. The highest power factor $S^2\sigma = 2{,}04 \times 10^{-4}$ W / cm K^2 at 1006 K was determined for the composition $CaMn_{0.90}Nb_{0.10}O_{3-\delta}$.

SEM images (Figure 1) reveal that the soft chemistry synthesis method produces nano-sized particles which agglomerate on top of each other.

The highest ZT value of $ZT_{1000K} = 0.19$ was reached at 3% Nb substitution. The molar fraction of oxygen in the sample was measured to be 2.85.

More research is required to investigate the effect of the material density on the thermal conductivity applying a single crystal of the same compound as a standard. Single crystals can be grown using the Floating Zone technique (Crystal System Corp).

Future research will also focus on the improvement of ZT by using different doping elements and/or producing thin films of the TE perovskite-type oxide materials.

References

[1] A.J Moulson, J.M. Herbert: **Electroceramics: Materials, Properties, Applications**, Second Edition, John Wiley & Sons, England, 2003.

[2] Bocher, L., M. H. Aguirre, et al.: **Chimie douce synthesis and thermochemical characterization of meso-porous perovskite-type titanate phases**, Thermochim. Acta, doi: 10.1016/j.tca.2007.02.013., 2007.

[3] Bocher, Laura: **Synthesis,structure, microstructure and thermoelectric properties of manganates** phases, Thesis, 2008.

[4] D.M. Rowe: **Thermoelectric Handbook: macro to nano**, Taylor&Francis Group, 2006.

[5] G.S. Nolas, J. Sharp, H.J. Goldsmid: **Thermoelectrics: Basic Principles and New Materials Developments**, Springer-Verlag Berlin, 2001.

[6] G. D. Mahan: **Good Thermoelectrics**, Solid State Physics, 51: 81-157, 1998.

[7] L. Bocher, M. H. Aguirre, D. Logvinovich, A. Shkabko, R. Robert, M. Trottmann, and A. Weidenkaff: Inorg. Chem., 47, 8077-8085, 2008.

[8] S. Ohta, H. Ohta, K.J. Koumoto: Ceram. Soc. Jpn., 114, 102– 105, 2006.

[9] M.P. Pechini: Patent. US 3330697, 1967.

[10] R.Robert: **Synthesis, structure and thermoelectric properties of Cobaltate phases**, ISBN 978-86624-367-5, 2007.

[11] R. Venkatasubramanian, E. Siivola, et al.: **Thin-film thermoelectric devices with high room-temperature figures of merit**, Nature, 413: 597-602, 2001.

[12] A. Weidenkaff: **Preparation and application of nanostructured perovskite phases**, Adv. Eng. Mater, 6(9): 709-714, 2004.

Appendix

Scientific output and publications in 2009

1. Aguirre, M. H., Logvinovich, D., Bocher, L., Robert, R., Ebbinghaus, S. G., Weidenkaff, A., High temperature thermoelectric properties of Sr_2RuYO_6 and Sr_2RuErO_6 double perovskite influenced by the structure and microstructure, *Acta Mat*., **57** (2009) 108-115.
2. Bocher L., Aguirre M.H., Robert R., Logvinovich D., Bakardjieva S., Hejtmanek J. and Weidenkaff, A., High-temperature stability, structure and thermoelectric properties of $CaMn_{1-x}Nb_xO_3$ phases, *Acta Mat*. **57** (2009) 5667-5680.
3. Robert, R., Logvinovich, D. Aguirre, M.H., Ebbinghaus, S.G., Bocher, L. and Weidenkaff, A., Crystal structure, morphology and physical properties of $LaCo_{1-x}Ti_xO_3$ perovskites prepared by a citric acid assisted soft chemistry synthesis, *Acta Mat*., **58** (2010) 680-691.
4. Robert, R., Bocher, L., Aguirre, M. H. and Weidenkaff, A., Thermoelectric properties of *p*- and *n*-type oxide phases prepared by soft chemistry, *J. Appl. Energy*, accepted (2009).
5. Weidenkaff, A., Aguirre, M., Bocher, L., Trottmann, M., Tomes, P., and Robert, R., Development of perovskite-type cobaltates and manganates for thermoelectric oxide modules, *J. Korean Cer. Soc*., **47** online DOI:10.4191/KCERS. 20 1 0. 4 7 .1.000 (2010).